Coupling of geometric confinement and magnetic confinement in $In_{0.09}Ga_{0.91}As$/GaAs quantum wells in magnetic fields with varying orientations

M. Bayer, A. A. Dremin,* V. D. Kulakovskii,* A. Forchel, and F. Faller

Technische Physik, Universität Würzburg, D-97074 Würzburg, Germany

P. A. Knipp

Department of Physics and Computer Science, Christopher Newport University, Newport News, Virginia 23606

T. L. Reinecke

Naval Research Laboratory, Washington, D.C. 20375

(Received 19 May 1995)

High excitation photoluminescence investigations of a 30-nm-wide $In_{0.09}Ga_{0.91}As$/GaAs quantum well have been performed in magnetic fields up to $B = 10$ T with varying orientations and have been compared with the results of detailed numerical calculations. The coupling between the quantum-well confinement potential and the magnetic confinement potential is controlled by the tilt angle ϑ of the magnetic field relative to the quantum-well growth direction. For magnetic fields normal ($\vartheta = 0$) and parallel ($\vartheta = 90°$) to the quantum-well plane the two confinement potentials are decoupled. In parallel orientation the magnetic quantization enhances only the geometric one. With increasing magnetic field the length scale that determines the quantization changes from the quantum-well width to the magnetic length. In contrast, in a normal magnetic field, B induces, independently of the geometric quantization, the in-plane Landau quantization. Spectral lines arising from intersubband transitions between Landau levels of different quantum-well subbands cross each other when they come close. For all other field orientations the two confinement potentials are coupled. This coupling generates hybridized electronic levels, in which both geometric and magnetic quantization are mixed. Transitions involving levels of different symmetry cross, whereas transitions involving levels of the same symmetry anticross when they approach each other. In addition, the number of strongly allowed transitions is increased near the anticrossing regime due to the exchange of character between the levels.

I. INTRODUCTION

During the last two decades quasi-two-dimensional semiconductor heterostructures have been the subject of intense investigations of their basic physical properties and also of research work with respect to their technological applications. High magnetic fields are a particularly powerful tool for the investigation of the electronic states because the properties of the electron gas in a quantum well are strongly changed by the field.[1] Magnetotransport and magneto-optical studies have revealed important information about the electronic properties of two-dimensional structures. Whereas tilted magnetic fields are frequently used in transport studies as, for example, in the investigation of the quantum hall effect,[2-6] relatively few such optical experiments have been reported up to now, most of them in the far infrared.[7-11]

In a weakly excited quantum well at low temperature electrons and holes exist as excitons. The electron-hole interaction couples states of different subbands. This coupling leads to anticrossing phenomena when two levels of the same symmetry approach each other.[12-14] However, in dense electron-hole plasmas the electron-hole correlations are strongly suppressed by screening effects. Therefore interband transitions in optical experiments at sufficiently large carrier densities can be discussed in terms of electron-hole transitions.

In the present work we report on high excitation photoluminescence experiments on a 30-nm-wide, undoped $In_{0.09}Ga_{0.91}As$/GaAs quantum well in magnetic fields up to $B = 10$ T. The variation of the magnetic field orientation relative to the quantum-well growth direction as shown schematically in Fig. 1 has enabled us to study the coupling between the geometric confinement potential of the quantum well and the magnetic confinement potential. The strength of this coupling depends on the tilt angle ϑ between the magnetic field and the normal to the
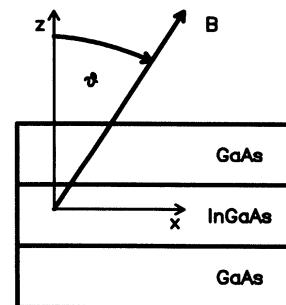

FIG. 1. Choice of the coordinate system for the gauge of the vector potential in Eq. (3) and definition of the tilt angle ϑ of the magnetic field relative to the quantum-well growth direction.

quantum-well plane. It varies continuously from a decoupled situation for an angle of $\vartheta = 0$ to maximum coupling for an angle of $\vartheta = 45°$ and is then again decreased to decoupling for an angle of $\vartheta = 90°$. The coupling results in a hybridization of geometrically and magnetically confined electronic states. Whereas hybridized states of the same symmetry anticross, when they approach each other, states of different symmetry do not interact and instead cross each other with varying B. This behavior can be seen in the magnetic field dependence of the interband transitions in the photoluminescence spectra. In addition, for tilted magnetic fields the symmetry of the levels is lowered in comparison to a field orientation normal to the quantum-well plane, which results in a reduction of the restrictions for allowed transitions imposed by selection rules and therefore in an increase of the number of optically observable transitions. The additional transitions are found to be strongest near the anticrossing regimes. Our experimental findings are compared with numerical calculations in which the full rectangular shape for the quantum-well confinement potential is considered in combination with the parabolic magnetic potential, which prevents for arbitrary field orientations an analytic solution of the problem. This is more realistic than using an approximate parabolic potential for the quantum well, which was done in most previous theoretical investigations.[15−20]

This paper is organized as follows: In Sec. II we give a description of the samples used in our investigations and also of the experimental setup. High excitation magnetoluminescence spectra for different tilt angles are presented in Sec. III and Sec. IV describes the theoretical model we have used to describe the experimental results. In Sec. V we discuss finally our experimental findings in comparison with our theoretical calculations. The results are summarized in Sec. VI.

II. EXPERIMENT

The heterostructure with a 30-nm-wide, strained $In_{0.09}Ga_{0.91}As/GaAs$ quantum well studied here was selected in order to provide a particularly simple band structure. The strain due to the lattice mismatch to the GaAs substrate causes a large heavy-hole–light-hole splitting of about 50 meV in $In_xGa_{1-x}As$ for the chosen quantum-well parameters so that the light-hole state is only weakly bound in the quantum well. Therefore the light-hole state lies well outside of the energetic region of interest in our investigations and, in addition, the influence of light-hole–heavy-hole band mixing can be neglected. Most importantly, the quantum-well width was chosen to be 30 nm so that the differences in energy between the subband energies and the cyclotron energies become comparable both for electrons and for holes in the range of magnetic fields available in our experiments. This allows us to study crossing and anticrossing between levels originating from different subbands at $B = 0$ with increasing magnetic field.

Photoluminescence experiments at a temperature of $T = 2$ K have been performed using an optical split coil magnetocryostat ($B < 10.5$ T). A cw Ar^+ laser (514.5 nm) was used for optical excitation. In order to observe emission from higher quantum-well subbands, electron-hole plasmas were generated by performing high excitation experiments with power densities of up to 10 $kW\,cm^{-2}$. The emitted light was dispersed by a 0.32-m single grating monochromator and detected by a liquid-nitrogen-cooled Si charge-coupled-device camera. In order to avoid problems due to density gradients quasi-two-dimensional plasmas were homogeneously excited in two-dimensional structures with an area of 50×50 μm^2. These quasi-two-dimensional structures were fabricated by electron-beam lithography and deep wet chemical etching. The samples could be rotated in the cryostat with an accuracy of $\pm 2°$.

III. HIGH EXCITATION SPECTRA

In contrast to photoluminescence excitation spectra of the investigated quantum well performed at low excitation powers, which provide a rich structure of spectral lines due to excited excitonic transitions with zero and nonzero angular momenta,[21] photoluminescence spectra of dense plasmas both without and with magnetic fields reveal a relatively small number of lines. Figure 2 shows a series of photoluminescence spectra for different excitation powers at zero magnetic field. For small excitation powers (lowest trace in Fig. 2) the spectrum consists of one line at about 1.43 eV, which can be attributed to excitonic recombination in the $m = 1$ electron and hole subbands, where m is the quantum number of the quantum-well confinement. With increasing laser power, up to three features appear subsequently in the spectrum. Our calculations show that there are three bound electron states and several bound heavy-hole states in the quan-
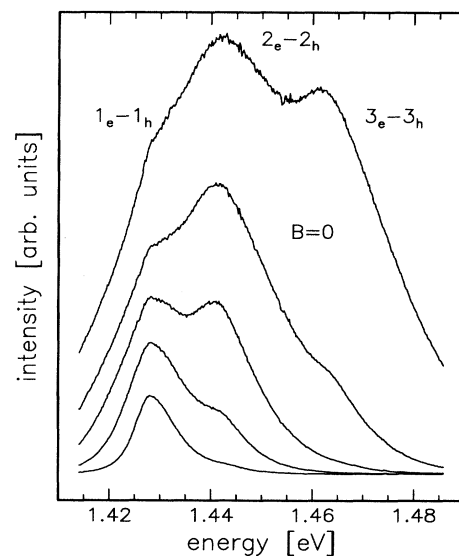

FIG. 2. Zero magnetic field spectra of the 30-nm-wide $In_{0.09}Ga_{0.91}As/GaAs$ quantum well for different optical excitation powers (from bottom to top, 0.4, 0.6, 0.8, 1.2, 1.6 $kW\,cm^{-2}$).

tum well. Therefore we can associate the three lines with transitions between the three electron levels in the quantum well and the three topmost valence subbands of the same quantum numbers, namely, the line at 1.427 eV with the 1_e-1_h transition, the line at 1.442 eV with the 2_e-2_h transition, and the line at 1.462 eV with the 3_e-3_h transition.

Figure 3 displays high excitation spectra at different magnetic fields for the tilt angles $\vartheta = 0$ and $\vartheta = 30°$ (excitation power: 2 kW cm^{-2}). Whereas the ground-state transitions show a very similar dependence on the magnetic field, the two excited transitions behave drastically different. While for normal orientation they cross each other, they anticross for tilted orientation, as indicated by the dashed-dotted lines. In detail, for both cases at fields $B < 6$ T and fields $B > 8$ T two well-separated spectral lines can be resolved that show nearly the same rates of increase of their energies with B: This increase is for one line approximately three times as large as that of the other one.

In between these two lines are still well separated for $\vartheta = 30°$. As they shift to higher energies with increasing B, they approach each other and come closest around $B = 7$ T, but always remain well separated. For higher fields they move apart again. In contrast, for $\vartheta = 0$ around $B = 7$ T only one very narrow spectral line can be resolved with twice the intensity and with a linewidth that is almost identical with the linewidths of the two well-separated lines for smaller or higher magnetic fields. For both tilt angles the relative intensities of the spectral lines change drastically with B. Whereas the spectral features show approximately equal intensity at low magnetic fields, with increasing fields the lower transitions become more and more pronounced and the ground-state transition clearly dominates. For normal magnetic fields this redistribution of oscillator strength is more pronounced than for the case of the tilted field.

Experiments have been also performed for magnetic fields parallel to the quantum well (excitation power 8 kW cm^{-2}). Typical spectra for this field orientation are displayed in Fig. 4. In contrast to all other field orientations the spectral lines at $B = 0$ do not split with increasing magnetic field. They remain broad for all fields available and the same qualitative exchange of oscillator strength between the transitions that we observed for the other field orientations is also observed here. At low magnetic fields the spectral lines shift only slightly to higher energies with increasing magnetic field. At large fields a distinct transition to a strong magnetic field dependence can be observed, especially for the two excited transitions.

IV. THEORY

Insight into the described behavior can be obtained from the Hamiltonian of a single particle in a quantum well under the influence of a magnetic field with arbitrary orientation relative to the quantum-well growth direction. As was shown earlier[21] for the 30-nm-wide quantum well studied in our experiments, excitonic effects are negligible already at plasma densities around 5×10^{11} cm^{-2} at $B = 4$ T. We therefore neglect them in our calculations, in which the typical plasma densities in all experiments can be estimated[22] to be always larger than 10^{12} cm^{-2}. In our coordinate system (see Fig. 1) the magnetic field is given by $B = (B_x, 0, B_z) = (B \sin\vartheta, 0, B \cos\vartheta)$. We orient the vector potential A to a point along the y axis. With this gauge choice the Hamiltonian can be written as

$$H = \tfrac{1}{2}(p_x^2 + p_z^2)/m$$
$$+ \tfrac{1}{2}m\omega_c^2(l_c^2 k_y + x \cos\vartheta - z \sin\vartheta)^2 + V(z) . \quad (1)$$

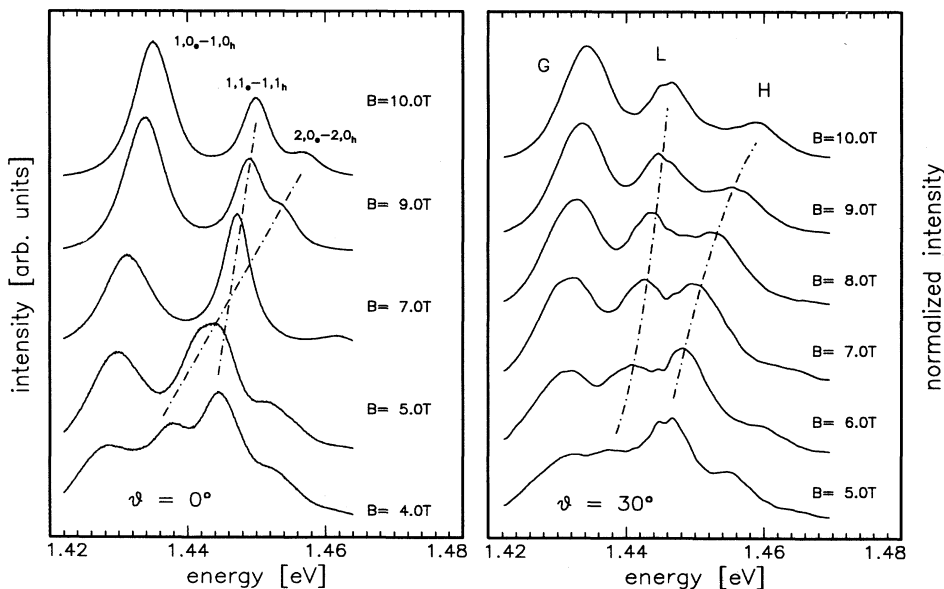Here $V(z)$ is the quantum-well potential. $\omega_c = eB/m$ is

FIG. 3. (a) High excitation spectra at different magnetic fields aligned normal to the quantum-well plane. The spectral lines of the 1,1e-1,1h transition and the 2,0e-2,0h transition cross each other as indicated by the dash-dotted lines. (b) High excitation spectra at different magnetic fields for a tilt angle of 30° of B relative to the quantum-well growth direction. The L transition and the H transition anticross. The two dashed-dotted lines are again guides for the eye. In both cases the excitation power was fixed at 2 kW cm^{-2}.
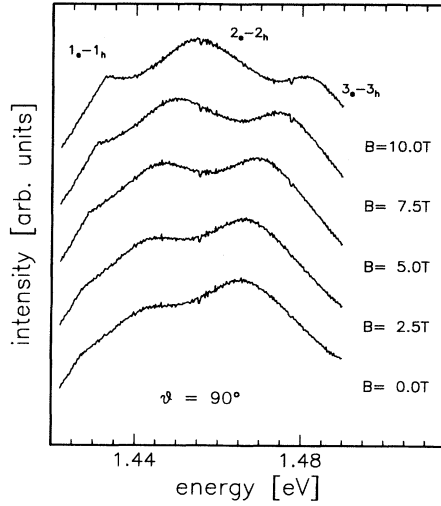
FIG. 4. Spectra at different magnetic fields with B parallel to the quantum-well plane (excitation power 8 kW cm^{-2}).

the cyclotron energy, and $l_c = \hbar^{1/2}/(eB)^{1/2}$ the magnetic length. Now the wave function can be written as

$$\Psi(x,y,z) = \exp(ik_y y)\psi(x,z) . \tag{2}$$

The wave number k_y affects the position of a state's reduced wave function ψ, but not its energy or its shape. The Hamiltonian (1) describes the motion of a particle in two potentials, the rectangular quantum-well potential perpendicular to the well plane and the harmonic magnetic potential perpendicular to both the magnetic field and the y direction. Both potentials are coupled by the term H_c in the magnetic potential, which mixes the x and z coordinates. H_c is controlled by the strength of the magnetic field and by the tilt angle ϑ:

$$H_c = -\tfrac{1}{2}m\omega_c^2 xz\sin2\vartheta . \tag{3}$$

The x and the z coordinates are decoupled for $\vartheta = 0$ and for $\vartheta = 90°$. In all other cases a coupling exists that is symmetric to $\vartheta = 45°$ in its strength, where it has maximum strength. As a result of the coupling of the potentials, Schrödinger's equation is in general no longer separable. Here we have calculated the eigenfunctions and eigenenergies by discretization of the Hamiltonian in the x,y coordinates and then by an iterative matrix diagonalization technique similar to that which we used earlier for the solution of the Hamiltonian for quantum wires and quantum dots.[23] The electron and hole in-plane masses were determined from the Landau-level splitting in perpendicular magnetic field. For the band offsets we used the values published in the literature.[24]

For arbitrary tilt angles there are two preferential directions in space that do not coincide except for $\vartheta = 0$, the quantum-well growth direction, and the magnetic field direction. For arbitrary tilt angles $\vartheta \leq 90°$ the electronic states can be categorized according to their behavior under rotations of 180° about the axis perpendicular to the two preferential directions, with our choice of the coordinate system about the y axis. The states can show either even symmetry or odd symmetry. Transitions are allowed only between states of the same symmetries and parities. Depending on the tilt angle the symmetry can be increased in comparison to arbitrary orientation.

V. DISCUSSION

A. Decoupled situation: Normal magnetic field

The orientation of the magnetic field normal to the quantum-well plane is the only orientation in which analytic solutions can be obtained, because the Schrödinger equation is separable. The geometric and the magnetic confinement potentials generate independently the vertical quantum-well quantization and the in-plane Landau quantization and the energy eigenvalues are given by

$$E = E_m + \hbar\omega_c(n + \tfrac{1}{2}) . \tag{4}$$

The levels can be consequently labeled m,n. Because of the independence of the two quantized energies, electron and hole Landau levels that originate from different quantum-well subbands cross each other, when they come close to each other.

The two preferential directions in space coincide for this field orientation. This leads to an increase of the symmetry of the states. The levels can be labeled according to the behavior under reflections along the quantum-well growth direction and along one direction normal to the magnetic field, with our gauge along the x direction. The combination of these two reflections is identical to the rotation of 180° around the y axis, which is the only symmetry for arbitrary field orientations. The allowed transitions m_e,n_e-m_h,n_h correspond therefore to interband transitions between the nth Landau level of the mth quantum-well electron subband and the nth Landau level of the mth quantum-well hole subband. In Fig. 3(a) we labeled the observed spectral lines accordingly.

The dependences of the transition energies on the magnetic field are shown in Fig. 5 in combination with the results of our theoretical calculations. At zero magnetic field three transitions can be seen. Landau fans rise from these subband transitions with increasing magnetic field. The diamonds denote the transition energies in magnetic field regimes where only one spectral line can be resolved. The determination of the transition energies below 4 T is impossible because of the splitting of the quantum-well subband transitions by the magnetic field into a large number of transitions between electronic levels, that are at $B < 4$ T too close in energy in order to separate them. Here and throughout the remainder of the paper the dashed lines denote levels (or spectral lines) of even symmetry with respect to the rotation of 180° about the y axis, the dotted lines those of odd symmetry.

As expected from the simple equation for the energy levels, crossing takes place for all observed spectral lines that originate from transitions between Landau levels of different subbands. The magnetic field at which the $1,2_e$-$1,2_h$ and the $2,1_e$-$1,2_h$ transitions cross ($B = 6.5$ T) is al-
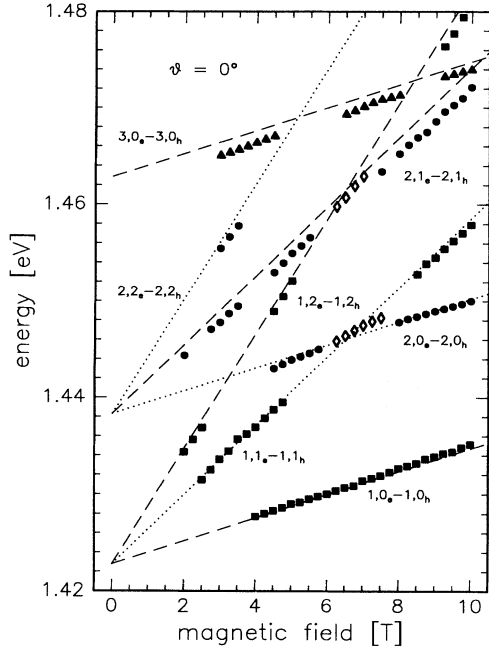
FIG. 5. Positions in energy of the observed intersubband transitions in a normal magnetic field. The open diamonds denote the position of the combined spectral line in field regimes where two lines are not separable. The dashed and dotted lines denote the calculated transition energies, either for even or for odd transition with respect to the 180° rotation about the y axis.

cause the interaction matrix elements between such states vanish. In our case both the electron and the hole levels, all of which contribute to the L and H emission lines, have odd symmetry with respect to the 180° rotation around the y axis. The positions in energy of the spectral lines near the anticrossing regime for $\vartheta = 30°$ are shown in Fig. 6 in combination with the results of our theoretical calculations for the transition energies. The anticrossing occurs at $B = 6.5$ T.

To determine the influence of the coupling term in general, H_c can be thought of as a perturbation. The symmetry of the unperturbed Hamiltonian (equivalent to the case $\vartheta = 0$) is higher than the symmetry of the total Hamiltonian, as described in the previous subsection. Far from the crossings, where the energies of the two levels are well separated, nondegenerate perturbation theory can be used. In these regimes each state includes only a small admixture of the other state and therefore shows nearly definite symmetry character; in our case, for example, the L_e state includes only a small contribution of the (2,0) state, and the H_e state includes only a small contribution from the (1,1) state and equivalently for the hole states L_h and H_h. That is, for B far below the resonance the L_e state can to a good approximation be labeled $1,1_e$, whereas the H_e state an be labeled $2,0_e$.

During anticrossing these states effectively exchange their character as seen from their dependence on the magnetic field. As a consequence, the L_e state, which shows a stronger B dependence for magnetic fields < 6 T, shows a weaker dependence on B for magnetic fields > 8
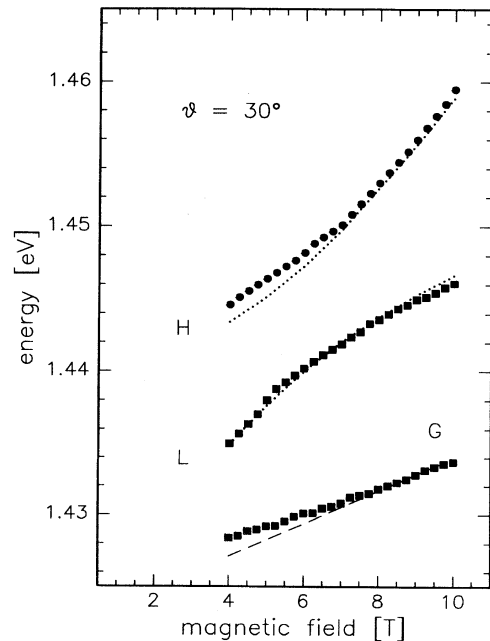
most identical with that at which the $1,1_e$-$1,1_h$ and the $2,0_e$-$2,0_h$ transitions cross. In contrast, that of the $1,2_e$-$1,2_h$ transition and of the $2,0_e$-$2,0_h$ transition lies near half of that magnetic field ($B = 3$ T). The crossing of the $1,2_e$-$1,2_h$ and of the $3,0_e$-$3,0_h$ transitions appears at approximately $B = 8.5$ T.

B. Coupled situation: Tilted magnetic field

In contrast to the case of normal magnetic field the spectral lines L and H, which correspond to the transitions $1,1_e$-$1,1_h$ and $2,0_e$-$2,0_h$, anticross for $\vartheta = 30°$. This is a result of the coupling of the magnetic and the geometric confinement potentials. This coupling causes a hybridization of the electronic levels: levels that arise from the two confinement potentials are now mixed, i.e., their energies can be no longer split into separate parts that arise from geometric and magnetic confinement.

Such an anticrossing behavior, which arises from the coupling between the two confinement potentials, is well known for systems in which the dispersion relations cross in the decoupled situation (see $\vartheta = 0$). In our case these dispersions correspond to the dependences of the electron and hole energies on the magnetic field. The inclusion of the interaction removes the degeneracy at the crossing points and causes a repulsion of the dispersions.

Anticrossing can occur only between states of the same symmetry, whereas states of different symmetry cross, be-

FIG. 6. Energies of the intersubband transitions in tilted magnetic field ($\vartheta = 30°$). The anticrossing of the L transition and the H transition occurs around $B = 7$ T. Dashed and dotted lines indicate again either even or odd transitions.

T (vice versa for the H_e transition). Therefore far above the resonance the L_e state can be denoted $2,0_e$ and the H_e state can be denoted $1,1_e$. Thus both states are approximately pure states $(1,1)$ and $(2,0)$ far from the resonances because of the only weakly broken reflection symmetries in these regimes. Therefore only two transitions are strongly allowed in these regimes, the L_e-L_h and the H_e-H_h transitions, because the restrictions for allowed transitions imposed by selection rules are effectively enhanced: Only transitions between states of the same x parity and of the same z parity are strongly allowed.

Near the resonances, degenerate perturbation theory has to be used. The two states that diagonalize the perturbation H_c in the subspace of unperturbed degenerate levels are strong mixtures of the two unperturbed states. For example, in the case of the electrons L_e and H_e are given by

$$|L_e\rangle \approx a_{11}|1,1_e\rangle + a_{12}|2,0_e\rangle \ ,$$

$$|H_e\rangle \approx a_{21}|1,1_e\rangle + a_{22}|2,0_e\rangle \ ,$$

$$a_{ij}=a_{ij}(B), \quad i,j=1,2 \ . \tag{5}$$

Because of the mixing of the unperturbed states in the anticrossing regime the number of transitions is increased with all four combinations of interband transitions being strongly allowed, i.e., besides the L_e-L_h and the H_e-H_h transitions two more, the L_e-H_h and the H_e-L_h, transitions show large oscillator strengths. The results of the numerical calculations for these four transitions are displayed in Fig. 7. In Figs. 7(a) and 7(b) the theoretical results for the electron and hole energy levels are shown and Fig. 7(c) shows the sums of the allowed electron-hole

transitions. The energy scale gives the contributions of the quantum-well potential and of the magnetic potential.

Whereas the electron mass is nearly isotropic, the hole masses in the calculations vary significantly with the spatial direction. In particular the hole mass along the z direction is significantly larger than the in-plane mass. Therefore one expects the anticrossing of the hole levels at smaller magnetic fields than the anticrossing of the electron levels. This is seen in the calculations. In Fig. 8(a) the differences in energy between the L and the H levels for electrons and for holes are shown. While the hole levels come closest ≈ 5 T, the electron levels anticross at higher fields ($B \approx 6$ T). However, when both contributions to the transition energies are added, the two anticrossings cannot be resolved separately, and the combined anticrossing appears over the whole range $B \approx 5$–6 T, as can be seen from Fig. 8(b), where we plotted the difference between the transition energies. The full circles display the experimentally measured difference in comparison with calculated differences of the transition energies of the L and of the H lines. An anticrossing magnetic field of about 6 T can be determined from both the theory and the experiments.

The intensities of the several transitions are expected to vary significantly as we pass through the anticrossing region due to wave-function mixing. These intensities are given by the squared transition matrix elements, for which the wave functions were calculated. The electron wave functions for a tilt angle of 30° at different magnetic fields ($B =4$, 7, and 10 T) for the L_e level and the H_e level are shown as contour plots in Fig. 9.[25] The nodal planes of these two states are perpendicular to each other for all magnetic field strengths. At slightly smaller magnetic
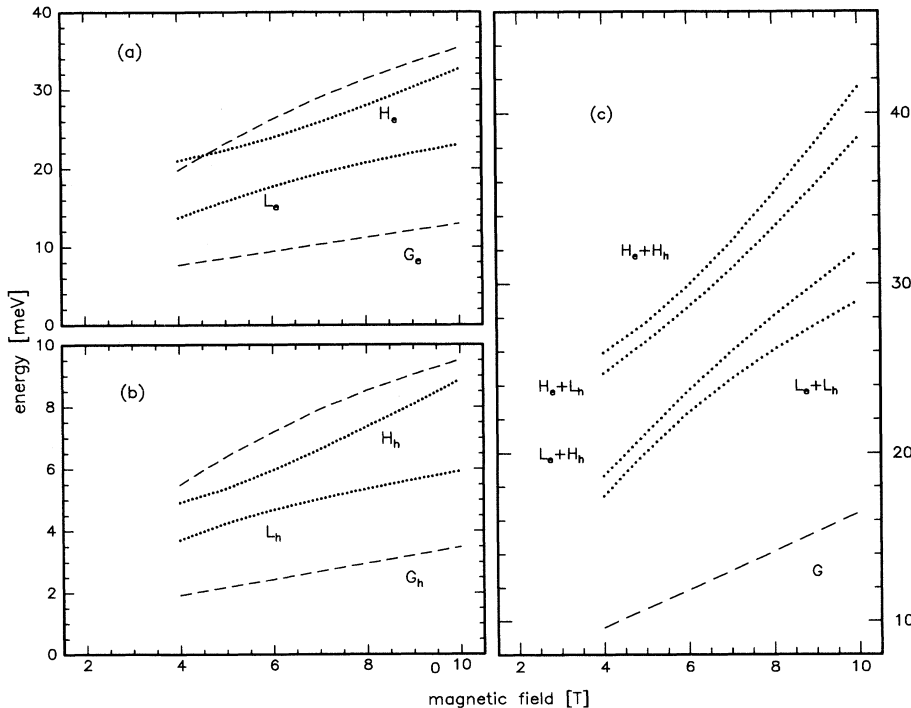

FIG. 7. Calculated energies of the electrons (a) and of the holes (b) for a tilt angle $\vartheta = 30°$. The energy scale shows only the contribution of the geometric and magnetic confinement potentials to the carrier energies. (c) The sum of the electron and hole energies for all four allowed transitions. The dashed lines display the energies of even states, the dotted lines those of odd states.
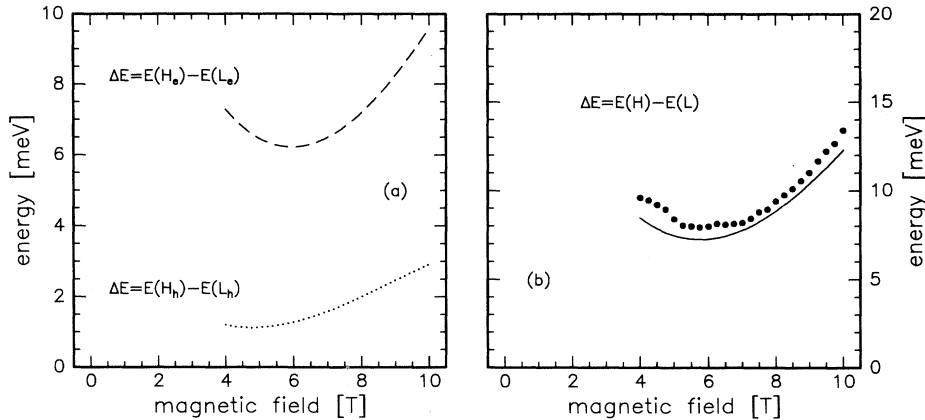
FIG. 8. (a) The difference in energy between the L and the H electron and hole levels. The differences between the L and H transition energies are plotted in (b) (solid line for the theoretically calculated energy difference; full circles for the experimentally measured).

fields than 4 T the nodal plane of the L_e wave function is parallel to the quantum-well growth direction, whereas the nodal plane of the H_e wave function is parallel to the quantum-well plane. The wave functions are rotated continuously by the increasing magnetic field, from $B = 0$ to 10 T by about 45°. At even higher fields the nodal planes of the two states are rotated by 90°, as expected by the exchange of character between the two states. In addition, it can be seen that both states are strongly localized in the quantum well with increasing magnetic field.

With these wave functions the transition matrix elements have been calculated, which are shown in Fig. 10. The matrix element of a transition is the square of the overlap integral of the corresponding normalized electron and hole (envelope) wave function:

$$|\langle \psi_h | \psi_e \rangle|^2 = |\int dx\, dz [\psi_h^*(x,z)\psi_e(x,z)]|^2 = f(B) . \qquad (6)$$

One can see in Fig. 10 that the matrix elements of the L_e-H_h and the H_e-L_h transitions are significantly different from zero only in the anticrossing regime from

$B = 6$ to 8 T, where an exchange of oscillator strengths takes place. Outside of that region the L_e-L_h transition and the H_e-H_h transitions clearly dominate. Therefore we expect to resolve only two spectral lines outside this regime, in which the L and the H electron and hole levels are involved, whereas the number of allowed transitions is to be doubled in the anticrossing regime, as expected from the previous qualitative discussion.

However, in the spectra only two lines can be seen. We attribute this in part to the fact that the transition matrix elements of the L_e-H_h and the H_e-L_h transitions are nearly one order of magnitude smaller than of the L_e-L_h and the H_e-H_h transitions in the anticrossing regime, and therefore the intensities of these transitions are much weaker. In addition, we attribute it to the rather small hole splittings. This causes two of the four transitions, which are different from each other only in the hole level spacing, not to be observable and the two corresponding spectral lines to be smeared out to effectively one line. Thus we argue that the L_e-L_h and the L_e-H_h transitions contribute to the spectral line that we labeled L and that
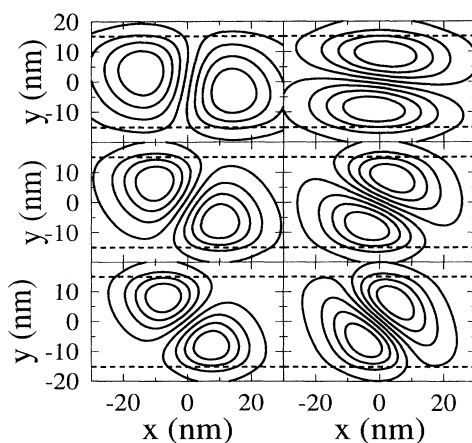

FIG. 9. Contour plots of the L_e (left) and of the H_e (right) electron wave functions at $B = 4$ T (top), 7 T (middle), and 10 T (bottom) for $\vartheta = 30°$.
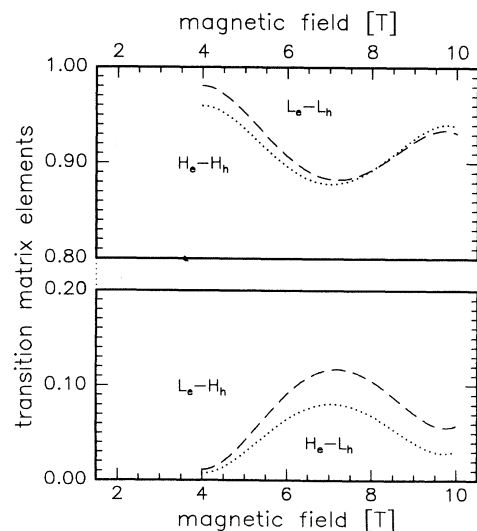

FIG. 10. Calculated transition matrix elements for the four allowed transitions between the L and H electron and hole levels as functions of the magnetic field for $\vartheta = 30°$.

the other two allowed transitions form the H spectral line.

To investigate the problem of the expected doubling of the number of spectral lines in the anticrossing regimes in more detail we have reduced the tilt angle to $\vartheta = 15°$. From one point of view this reduces the coupling H_c between the two confinement potentials. On the other hand the differences in energy between the levels is also decreased, leading to an enhanced interaction. The obtained experimental results are presented in Fig. 11. We observe two avoided crossings, one anticrossing between the L_1 and the H_1 spectral lines at $B = 7.5$ T and another anticrossing between the L_2 and the H_2 spectral lines at $B = 7$ T. In addition we observe a crossing between the H_1 and the L_2 transitions at $B = 3.5$ T. The L_2 and the H_1 transitions cross because of their different symmetry. On the other hand, the L_1 and the H_1 transitions and the L_2 and the H_2 transitions anticross because they have the same symmetry.

As seen in Fig. 12 for a magnetic field of 9.5 T, in contrast to the case of $\vartheta = 30°$, for B higher than those for which the anticrossing occurs, three lines can be resolved in the spectra for $\vartheta = 15°$ that are positioned in the energy range of the two lower anticrossing transitions (excitation power 2 kW cm^{-2}). Three features now appear at about 1.450 eV, at about 1.454 eV, and at about 1.458 eV. The central spectral M line is very intense in the anticrossing regime, but loses intensity rather quickly with increasing magnetic field. Vice versa, the intensities of the two
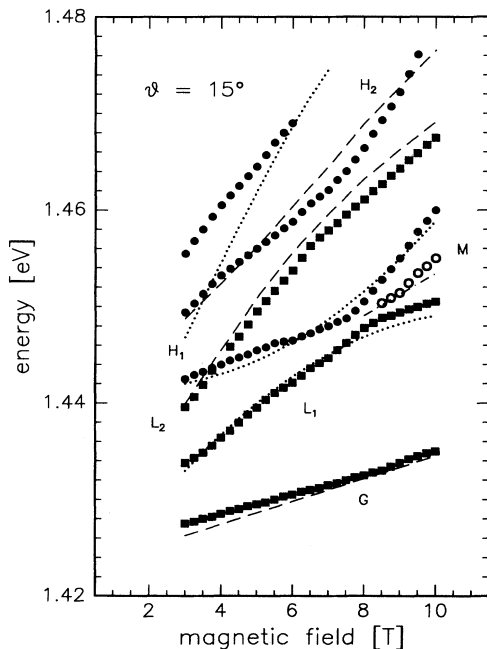

FIG. 12. Photoluminescence spectrum recorded at $B = 9.5$ T for the tilt angle of $\vartheta = 15°$. Only the part of the spectrum near the anticrossing regime is shown. Three spectral lines are clearly resolvable; the lines corresponding to the L_{1e}-L_{1h} and the H_{1e}-H_{1h} transitions and a mixed line to which both the L_{1e}-H_{1h} and the H_{1e}-L_{1h} transitions contribute.

FIG. 11. Positions in energy of the spectral lines for a tilt angle of $\vartheta = 15°$. Two avoided crossings are observed, between the L_1 and the H_1 transitions and between the L_2 and H_2 transitions. In contrast the L_2 and the H_1 transitions cross each other. An additional feature denoted by M is observed around 8.5 T. The lines denote the calculated transition energies.
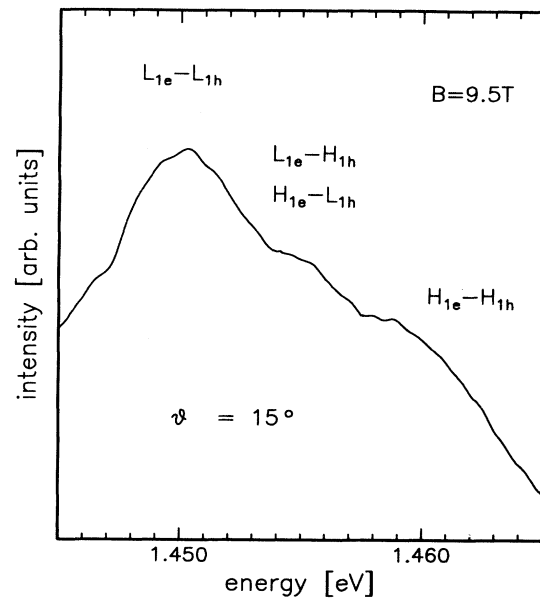
outer transitions are rather weak at 8.5 T, but they are already dominant at 9.5 T. This observation of three lines arises from the theoretically expected four transitions in the anticrossing regime. We attribute the inner spectral line to the two transitions L_{1e}-H_{1h} and H_{1e}-L_{1h} that are weak outside the anticrossing regime. Here they cannot be resolved separately but are smeared out to one spectral feature. The L_{1e}-L_{1h} and H_{1e}-H_{1h} transitions, which are the only allowed ones outside the anticrossing regime, can be assigned to the two outer transitions.

In contrast to $\vartheta = 30°$ this feature can be detected in the spectra for $\vartheta = 15°$, because the oscillator strengths of the contributing transitions shown in Fig. 13 in the anticrossing regime are now of the same order of magnitude as those of the two transitions between the L_1 electron and L_1 hole levels and the H_1 electron and the H_1 hole levels. This is due to the decreased energy splitting between the anticrossing states in comparison to the case of the angle of 30°, which enhances the interaction between the levels. To obtain also a qualitative impression how the electron (solid lines) and the hole (dotted lines) wave functions affect the transition matrix elements contour plots of the overlap of the L_{1e} wave function with both the L_{1h} and the H_{1h} wave functions are shown in Fig. 14 at different magnetic fields over the entire anticrossing regime ($B = 5$, 6, 7, and 8 T). One can clearly see how the overlap of the two wave functions varies strongly with increasing magnetic field resulting in such strongly varying oscillator strengths.

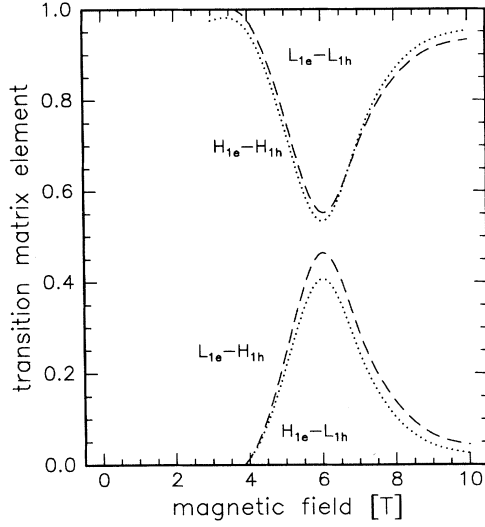In addition we calculated the averaged energy of the

FIG. 13. Transition matrix elements of the four allowed transitions between the L_1 and the H_1 electron and hole levels. The matrix elements for the L_{1e}-H_{1h} and the H_{1e}-L_{1h} transitions are of the same order of magnitude as those of the L_{1e}-L_{1h} and the H_{1e}-H_{1h} transitions.

L_{1e}-H_{1h} and the H_{1e}-L_{1h} transitions to obtain the energy of the M transition. More precisely, we have calculated the transition energy as the sum of energies of each of the electron states with the corresponding hole state weighted by the square of the corresponding electron-hole matrix elements:

$$E_M = (|\langle H_{1h}|L_{1e}\rangle|^2/N)E(L_{1e}\text{-}H_{1h})$$

$$+ (|\langle L_{1h}|H_{1e}\rangle|^2/N)E(H_{1e}\text{-}L_{1h}) , \qquad (7a)$$

$$N = |\langle H_{1h}|L_{1e}\rangle|^2 + |\langle L_{1h}|H_{1e}\rangle|^2 . \qquad (7b)$$

These energies are already shown by the dashed line in Fig. 11. The energy of the M transition lies approximately in the middle of the energies of the L_{1e}-L_{1h} and of the H_{1e}-H_{1h} transitions.

Between $B = 8$ and 10 T we have made also a detailed line-shape analysis of the luminescence lines arising from the lower anticrossing transitions to determine the integrated intensity of these transitions.[26] Assuming that the involved levels are completely filled with carriers, these intensities should reflect the magnitudes of transition matrix elements. The total intensity of all four anticrossing transitions increases with increasing magnetic field due to the increase of the number of electronic states in each quantized level with increasing B. The integrated intensities of the three measured spectral lines L_1, M, and H_1 are presented in Fig. 15. While the M line dominates at $B = 8$ T and is approximately twice as strong as each of the two other transitions, its intensity decreases continuously with increasing B and is about one order of magnitude smaller than the intensities of the L_1 and H_1 spectral lines for higher fields. This is roughly what is expected by the theoretical calculations of the transition matrix elements.

Both for normal ($\vartheta = 0$) and for tilted ($0 < \vartheta \leq 90°$) field orientation the energy levels are fully quantized and are highly degenerate with respect to k_y, the wave vector along the y direction. The degree of degeneracy g is proportional to the magnetic field component normal to the quantum-well plane, $B \cos\vartheta$:

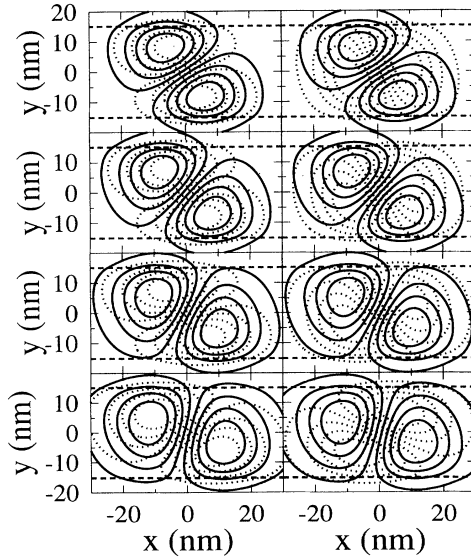$$g = 4.838 \times 10^{10} \text{ cm}^{-2}(B \cos\vartheta)/T . \qquad (8)$$

FIG. 14. Contour plots of the overlaps of the lowest anticrossing electron level L_{1e} with the two lowest anticrossing levels L_{1h} (left) and H_{1h} (right) for $B = 5$, 6, 7, and 8 T (from bottom to top) for $\vartheta = 15°$.

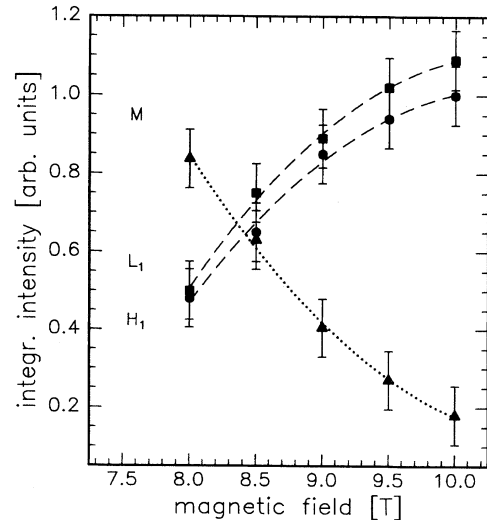FIG. 15. Integrated luminescence intensities of the three experimentally observed spectral lines L_1, M, and H_1 for the tilt angle of $\vartheta = 15°$.

Therefore the number of states increases linearly with B and carriers are redistributed from higher to lower states. This explains the behavior of the relative intensities in Figs. 3(a) and 3(b). The intensity of the ground-state emission is drastically enhanced relative to the excited transitions with increasing magnetic field. This pronouncement is stronger the smaller the tilt angle ϑ is, because of the angle dependence of g.

C. Decoupled situation: Parallel magnetic field

For the field direction parallel to the quantum-well plane the two confinement potentials are again decoupled. With the gauge in Eq. (3) for the vector potential they combine to a potential that is one dimensional in the z direction. The magnetic potential enhances mainly the geometric one and hence a splitting of the quantum-well subbands with increasing magnetic field is prevented.

The geometric confinement dominates the levels for small magnetic fields, whereas the magnetic confinement potential dominates for high fields. In detail, at small B the quantum-well width is the length scale that determines the quantization of the carriers. With increasing magnetic field the magnetic confinement becomes more and more important, since the extension of the wave function is decreased. At high fields finally the magnetic length is significantly smaller than the quantum-well width and determines the carrier quantization. Consequently the energies of the levels change from a B^2-dependent diamagnetic shift at weak fields to a linear dependence on B at high fields. The regimes of low and high fields are defined by the relation between the quantum-well width L_z and the magnetic length l_c. The changeover takes place when both length scales become comparable.

This behavior is reflected in our experiments, as can be seen in Fig. 16, where the experimentally determined transition energies are displayed as functions of the magnetic field in combination with the results of our numerical calculations. The changeover takes place around 6 T and the high-field behavior of the transition energies is the stronger the higher the subband index is.

The parallel magnetic field orientation is also different from all the other field orientations because the energy levels are not fully quantized due to the free dispersion along B. This dispersion causes the large linewidths of the spectral lines in contrast to the comparatively small linewidths for $\vartheta < 90°$. Whereas the density of states for the other field orientations changes from a quasi-two-dimensional behavior (delta-function-like) to a quasi-zero-dimensional behavior in magnetic field, the density of states for parallel orientation changes to a quasi-one-dimensional behavior $(E - E_m)^{-1/2}$-function-like). Nevertheless the number of states on a subband increases also with B and therefore again a redistribution of carriers from higher to lower subbands takes place, which explains the change of the relative intensities in Fig. 4.
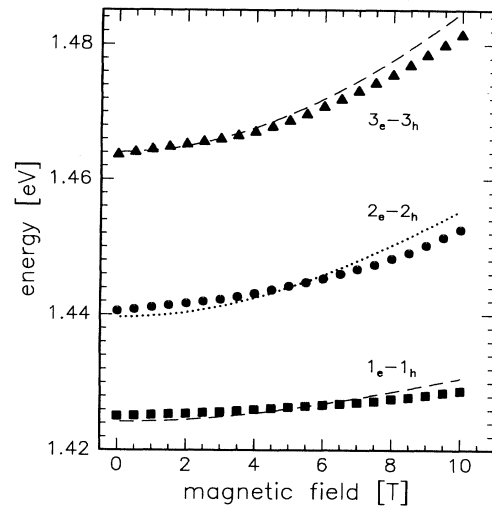

FIG. 16. Energies of the observed intersubband transitions in parallel magnetic field. The calculated transition energies are shown as lines, where the dashed lines denote transitions that are even with respect to a rotation of 180° about the y axis and the dotted line denotes an odd transition.

VI. SUMMARY

In conclusion, we have investigated the influence of the coupling of the geometric confinement potential and the magnetic confinement potential in a 30-nm $In_{0.09}Ga_{0.91}As/GaAs$ quantum well by tilting the magnetic field out of the growth direction. In this way we have varied the strength of the coupling from a decoupled situation $(\vartheta = 0)$ over coupled situations (at $\vartheta = 30°$ and $\vartheta = 15°$) again to decoupling $(\vartheta = 90°)$. For tilt angles $0 < \vartheta < 90°$ this coupling leads to an anticrossing of electronic energy levels of the same symmetry, while states of different symmetry cross. This behavior is reflected in the photoluminescence spectra and is typical for interacting systems with crossing dispersion relations in the uncoupled case. In the anticrossing regimes the number of allowed transitions is doubled. We found clear indications for the doubling of these lines. In magnetic fields parallel to the quantum-well plane the magnetic field primarily causes an enhancement of the quantum-well confinement potential that increases the subband spacing. The evolution of Landau fans out of these subbands does not occur and the motion along the magnetic field in the quantum-well plane remains free for all field strengths.

ACKNOWLEDGMENTS

*On leave from the Institute of Solid State Physics, Russian Academy of Sciences, 142432 Chernogolovka, Russia.

[1] An overview is given, for example, in *High Magnetic Fields in Semiconductor Physics I*, edited by G. Landwehr, Springer Series in Solid State Sciences Vol. 71 (Springer-Verlag, Berlin, 1987); *High Magnetic Fields in Semiconductor Physics II*, edited by G. Landwehr, Springer Series in Solid State Sciences Vol. 87 (Springer-Verlag, Berlin, 1989); *High Magnetic Fields in Semiconductor Physics III*, edited by G. Landwehr, Springer Series in Solid State Sciences Vol. 101 (Springer-Verlag, Berlin, 1992).

[2] T. Englert, K. von Klitzing, R. J. Nicholas, G. Landwehr, G. Dorda, and M. Pepper, Phys. Status Solidi B **99**, 237 (1980).

[3] R. J. Haug, K. von Klitzing, R. J. Nicholas, J. C. Maan, and G. Weimann, Phys. Rev. B **36**, 4528 (1987).

[4] W. Heuring, E. Bangert, G. Landwehr, G. Weimann, and W. Schlapp, in *High Magnetic Fields in Semiconductor Physics II* (Ref. 1), p. 190; M. Kraus, H. Mrotzek, N. Steinmetz, E. Bangert, and G. Landwehr, *ibid.*, p. 194.

[5] R. G. Clark, S. R. Haynes, A. M. Suckling, J. J. Harris, and C. T. Foxon, Phys. Rev. Lett. **62**, 1536 (1989); R. G. Clark, S. R. Haynes, J. V. Branch, A. M. Suckling, P. A. Wright, P. M. W. Oswald, J. J. Harris, and C. T. Foxon, Surf. Sci. **229**, 25 (1990).

[6] J. P. Eisenstein, H. L. Störmer, L. Pfeiffer, and K. W. West, Phys. Rev. Lett. **62**, 1540 (1989); Phys. Rev. B **41**, 7910 (1990).

[7] W. Beinvogl, A. Kamgar, and J. F. Koch, Phys. Rev. B **14**, 4274 (1976).

[8] Z. Schlesinger, J. M. C. Hwang, and S. J. Allen, Phys. Rev. Lett. **50**, 2098 (1983).

[9] M. Zaluzny, Solid State Commun. **55**, 747 (1985); **56**, 235 (1985).

[10] S. Huant and G. Martinez, Superlatt. Microstruct. **6**, 103 (1989); S. Huant, G. Martinez, and B. Etienne, Europhys. Lett. **9**, 397 (1989); S. Huant, M. Grigenberg, G. Martinez, and B. Etienne, Solid State Commun. **65**, 457 (1988).

[11] K. Karrai, H. D. Drew, M. W. Lee, and M. Shayegan, Phys. Rev. B **39**, 1426 (1989).

[12] L. Vina, G. E. W. Bauer, M. Potemski, J. C. Maan, E. E. Mendez, and W. I. Wang, Phys. Rev. B **41**, 10 767 (1990).

[13] G. E. W. Bauer and T. Ando, Phys. Rev. B **38**, 6015 (1988).

[14] V. D. Kulakovskii, B. N. Shepel, K. Pieger, J. Straka, B. N. Shepel, and S. V. Nochevny, Phys. Rev. B **50**, 7467 (1994).

[15] J. C. Maan, in *Two-Dimensional Systems, Heterostructures, and Superlattices*, edited by G. Bauer, F. Kuchar, and H. Heinrich, Springer Series in Solid State Sciences Vol. 53 (Springer-Verlag, Berlin, 1984), p. 183.

[16] R. Merlin, Solid State Commun. **64**, 99 (1987); R. Borroff, R. Merlin, R. L. Green, and J. Comao, Superlatt. Microstruct. **3**, 493 (1987).

[17] T. Chakraborty and P. Pietilaeinen, Phys. Rev. B **39**, 7971 (1989); **41**, 10 862 (1990).

[18] T. Ando, Z. Phys. B **26**, 263 (1977); J. Phys. Soc. Jpn. **50**, 2978 (1981); T. Ando, A. B. Fowler, and F. Stern, Rev. Mod. Phys. **54**, 437 (1982).

[19] G. Bastard, *Wave Mechanics Applied to Semiconductor Hetero-structures* (Les Editions de Physique, Les Ulis, 1988).

[20] G. Marx, K. Lier, and R. Kümmel, in *High Magnetic Fields in Semiconductor Physics III* (Ref. 1), p. 180.

[21] M. Bayer, A. Dremin, F. Faller, A. Forchel, V. D. Kulakovskii, B. N. Shepel, and T. Andersson, Phys. Rev. B **50**, 17 085 (1994).

[22] The plasma density can be estimated from the number of completely and partially filled Landau levels in normal magnetic field ($\vartheta = 0$), since the number of states in one Landau level depends only on the magnetic field by the relation $N_{LL} = 4.838 \times 10^{10} B / T \, \mathrm{cm}^{-2}$.

[23] Ch. Gréus, L. Butov, F. Daiminger, A. Forchel, P. A. Knipp, and T. L. Reinecke, Phys. Rev. B **47**, 7626 (1993); M. Bayer, A. Forchel, I. E. Itskevich, T. L. Reinecke, P. A. Knipp, Ch. Gréus, R. Spiegel, and F. Faller, *ibid.* **49**, 14 782 (1994); M. Bayer, A. Schmidt, A. Forchel, F. Faller, T. L. Reinecke, P. A. Knipp, A. A. Dremin, and V. D. Kulakovskii, Phys. Rev. Lett. **74**, 3439 (1995).

[24] For the conduction band we used an offset of 55.5 meV, while for the valence band an offset of 29.9 meV was used. The electron mass was assumed to be isotropic and was taken to be 0.06315 in the quantum well and 0.0665 outside in the GaAs regions. The hole mass in the z direction was taken to be 0.35 in and outside of the quantum well and the lateral hole mass was assumed to be 0.10 in the barrier. As already mentioned the lateral hole mass in the well was adjusted to a value of 0.21.

[25] We do not show the electronic wave functions at even lower magnetic fields, because at small magnetic fields the H_e state undergoes avoided crossings with states of the same symmetry, that originate from the lowest quantum-well subband. For $B \neq 0$ these states can be labeled $1, (2n-1)e$.

[26] The line-shape analysis was performed by fitting three Gaussian lines corresponding to the L_1, the M, and the H_1 transitions to the spectra. In order to minimize the number of free fit parameters we took the positions in energy of the three spectral lines, that were determined in the experiment as the maxima of the Gaussian lines. The widths of the two outer lines were assumed to be identical and were taken to be equal to the linewidth of the ground-state transition. In addition also the intensities of the two outer transitions were assumed to be identical. For the analysis spectra there were recorded at very high excitation (10 kW cm^{-2}) were taken in order to ensure that the corresponding levels are fully occupied.